

Conditional Unscented Autoencoders for Trajectory Prediction

Faris Janjos¹ Marcel Hallgarten^{1,2} Anthony Knittel^{1,3} Maxim Dolgov¹ Andreas Zell² J. Marius Zöllner⁴

Abstract—The Conditional Variational Autoencoder (CVAE) is one of the most widely-used models in trajectory prediction for Automated Driving (AD). It captures the interplay between a driving context and its ground-truth future into a probabilistic latent space and uses it to produce predictions. In this paper, we challenge key components of the CVAE. We leverage recent advances in the space of the Variational Autoencoder (VAE), the foundation of the CVAE, which show that a simple change in the sampling procedure can greatly benefit performance. We find that unscented sampling, which draws samples from any learned distribution in a deterministic manner, can naturally be better suited to trajectory prediction than potentially dangerous random sampling. We go further and offer additional improvements including a more structured Gaussian mixture latent space, as well as a novel, potentially more expressive way to do inference with CVAEs. We show wide applicability of our models by evaluating them on the INTERACTION prediction dataset, outperforming the state of the art, as well as at the task of image modeling on the CelebA dataset, outperforming the baseline vanilla CVAE. Code is available at: <https://github.com/boschresearch/cvae-prediction>.

I. INTRODUCTION

Predicting the motion of human-driven vehicles sharing an environment with an autonomous system is a key enabler for fully-automated driving. Rich environment contexts present in urban driving and the prevalent interaction between traffic participants make it imperative to model the uncertainty in future trajectories. In this task of probabilistic trajectory prediction, machine learning models have proven indispensable. By learning a probability distribution, either in the space of the model’s internal representations or the model’s output, they capture the uncertainty inherent to the problem.

In addressing the challenges of probabilistic trajectory prediction, many approaches use established generative models such as a CVAE, a Generative Adversarial Network (GAN), or a Normalizing Flow (NF). The CVAE is especially useful; its powerful latent space model represents the underlying structure present in the relationship between a future trajectory and the potentially high-dimensional historical context that induces it. This real-world joint distribution is compressed into a tractable, relatively low-dimensional latent space Gaussian, amenable to sampling. Generating future predictions involves simply drawing samples from the latent space and transforming them into trajectories. The tasks of compressing inputs into the latent space and decompressing predictions from it are delegated to the CVAE’s encoder and decoder, which can leverage powerful GNN or Transformer models. Thus, it has been a method of choice in state-of-the-art probabilistic prediction [1], [2], [3], [4], [5], [6].

¹ Robert Bosch GmbH, Corporate Research, Renningen, Germany first-name.last-name@bosch.com; ² University of Tübingen, Tübingen, Germany; ³ Five AI Ltd, Cambridge, United Kingdom; ⁴ FZI Research Center for Information Technology, Karlsruhe, Germany

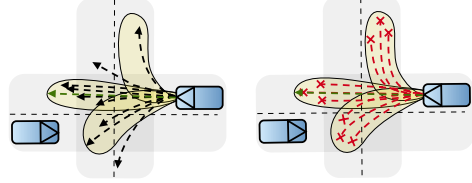


Fig. 1: Assume a trajectory predictor learned a multi-modal distribution (yellow), either by propagating its latent space or directly in the output space. Random sampling (black) can bring unsafe, unlikely, or in-between-mode outputs. In contrast, the unscented sampling (red), realized by computing sigma points of the distribution, brings structure to the learned stochasticity.

Despite its wide appeal, the CVAE has certain shortcomings when applied in trajectory prediction. It does not provide an out-of-the-box means to evaluate the likelihoods of its trajectories. Further, since the distribution of future motion is highly multi-modal (usually involving distinct behaviors), recovering it from a smooth Gaussian latent space used in continuous CVAEs can bring unreasonable in-between outputs. Finally, the randomness inherent to the model is at odds with the primacy of safety and reproducibility. Random sampling of the latent space in inference can generate spurious and potentially dangerous trajectories (see Fig. 1) as well as miss critical trajectories, in addition to bringing a high gradient variance in training (a pitfall of the VAE itself). This can have serious ramifications on a downstream planner fed CVAE-predicted futures; these might differ significantly over consecutive prediction calls. Overall, these issues can be traced back to the CVAE’s overly simplistic latent space and the unreliable random sampling.

Our work challenges well-established assumptions surrounding the CVAE and its Gaussian latent space. We aim to answer the following two research questions: (i) *Can the random sampling and propagation be replaced by more structured selection?*, (ii) *Are there effective alternatives to the simplistic latent space in training and inference, especially considering multi-modality of the output space?* In answering (i), we leverage recent advancements in the base VAE [7] while for (ii), we use more expressive distributions. As we improve core aspects of the CVAE, we also evaluate our models on image generation tasks. Our contributions are:

- Unscented sampling and transformation of CVAE distributions as an alternative to random sampling for trajectory prediction, tackling (i). As part of this contribution, we develop a novel Conditional Unscented Autoencoder (CUAE) model with deterministic sampling.
- A CVAE extension toward a mixture model latent space in place of a Gaussian latent space (usable with both random and unscented sampling). It promotes multi-modality in the output-space and tackles (ii).

- A novel approach for inference with CVAEs via conditional ex-post estimation, inspired by [7] and tackling (ii). It preserves latent space training but circumvents the need to use it in inference by building and sampling a more expressive distribution instead.

II. RELATED WORK

In the following, we discuss approaches to probabilistic trajectory prediction, i.e. modeling the conditional distribution $\mathcal{P}(\mathbf{y}|\mathbf{x})$ of future trajectories \mathbf{y} given a generic context \mathbf{x} . A popular choice is to represent $\mathcal{P}(\mathbf{y}|\mathbf{x})$ by a **set of trajectories**. Here, a fixed number of modes with associated probabilities is regressed either individually per agent [8], [9], [10], [11], [12] or jointly for all agents in a scene [13], [14], [15], [16], [17]. Commonly, winner-takes-all (WTA) loss functions only consider the predicted mode closest to the ground truth, exhibiting low sample efficiency. Moreover, as non-winner modes are not penalized, the predicted set can contain unrealistic and inadmissible trajectories (e.g. off-road). Many approaches address such issues by explicitly conditioning on map elements [18], [11], [19], [20], [21].

Other classes of models attempt to directly capture $\mathcal{P}(\mathbf{y}|\mathbf{x})$ into a **parametric distribution** such as a Gaussian Mixture Model (GMM). Here, trajectories are considered means of mixture components and (co)variances are learned separately [22], [23], [24], [25], [26]. This approach models the uncertainty of the underlying problem more accurately. Moreover, loss functions can consider the entire distribution (via the Negative Log Likelihood (NLL)), increasing sample efficiency and reducing inadmissible predictions. However, these models are theoretically limited since they do not reason about the generative process of the data, i.e. $\mathcal{P}(\mathbf{x}, \mathbf{y})$.

In contrast, **generative models** such as NFs [27], [28], [29], GANs [30], [31], [32], [33], [34], or CVAEs [1], [2], [3], [4], [5], [6], attempt to first learn a proxy for the joint data distribution and then obtain the predictive distribution $\mathcal{P}(\mathbf{y}|\mathbf{x})$. By sampling a prior and propagating the samples into the output space, they can implicitly capture rich non-parametric distributions. Among these models, NFs have limited expressiveness for high-dimensional data distributions found in trajectory prediction as well as strict architectural constraints, although they provide tractable likelihoods. Among GANs, prevalent issues include lack of diversity and mode collapse [35], out-of-distribution samples [36], [37], and training instability [38], [39]. Moreover, GANs learn a continuous transformation and are unable to model disconnected manifolds [36], [37], [40], which is often necessary in prediction. To mitigate this, [40] uses multiple generators.

Similarly, CVAEs can struggle to model output distributions with disconnected modes [41]. The decoder transformation is continuous and the latent distribution capturing multiple futures is commonly modeled as a multivariate Gaussian. The approaches in [2], [42] address the issue by using a discrete latent variable mapped to a GMM output, which also facilitates integration over the conditional prior distribution. However, this limits the expressiveness of the latent space. In this work, we approach this problem

by leveraging more expressive latent distributions such as GMMs in both training and inference. Furthermore, many models adapt the CVAE to output likelihoods by additional classifier networks, a common approach across the trajectory prediction landscape [3], [4], [26]. Another pitfall of CVAEs is that propagating the latent distribution to the output space involves drawing and decoding random samples. The randomness can result in bad coverage of the true output distribution, especially with few samples. To mitigate this, [4] and [5] employ diversity sampling techniques in training, while [4] off-loads the modeling of distinct futures to a GNN decoder. In inference, [4] uses only the latent mean and abandons the rich learned latent space. In contrast, we use deterministic sampling [7] to obtain diverse and representative samples from the learned latent space.

III. METHOD

We consider the task of modeling $\mathcal{P}(\mathbf{y}|\mathbf{x})$, where \mathbf{y} are future vehicle trajectories \mathbf{y} , i.e. a $T \times 2$ matrix of T future positions, and \mathbf{x} is a generic context. In addressing this task, we leverage the CVAE framework to construct and sample an expressive latent space. Thus, we outline the presentation of our approach along the research questions posed in Sec. I. Sec. III-A provides a CVAE background and proposes alternatives to random sampling and transformation of the latent space, tackling (i), while Sec. III-B offers alternatives in latent space modeling and using it for inference, tackling (ii). Sec. III-C discusses the generation of output trajectories given the choices in Sec. III-A and Sec. III-B.

A. Latent Space Sampling and Transformation

1) *CVAE Background*: CVAEs [43] are generative models that can capture a conditional distribution $\mathcal{P}(\mathbf{y}|\mathbf{x})$. They model the relationship between pairs of high-dimensional inputs \mathbf{x} and \mathbf{y} by projecting them into a lower-dimensional latent space \mathbf{z} , see Fig. 2. An encoder parameterized by ϕ learns the latent posterior distribution $q_\phi(\mathbf{z}|\mathbf{x}, \mathbf{y}; \boldsymbol{\mu}_\phi, \boldsymbol{\Sigma}_\phi)$, commonly modeled as a multivariate Gaussian. Then, a θ -parameterized decoder is tasked with estimating the true output distribution $\mathcal{P}(\mathbf{y}|\mathbf{x})$. This is done by conditioning on \mathbf{x} and drawing random samples \mathbf{z} from q_ϕ to first produce $p_\theta(\mathbf{y}|\mathbf{x}, \mathbf{z})$ and thus marginalize out \mathbf{z} . In inference, since the ground-truth \mathbf{y} is not available, the model instead samples a surrogate, γ -parameterized latent prior $p_\gamma(\mathbf{z}|\mathbf{x}; \boldsymbol{\mu}_\gamma, \boldsymbol{\Sigma}_\gamma)$. The posterior q_ϕ and prior p_γ are trained to be consistent. Thus, the loss function minimizes $\mathcal{L}_{\text{CVAE}} = \mathcal{L}_{\text{REC}} + \mathcal{L}_{\text{KL}}$ (and maximizes the Evidence Lower Bound (ELBO) [44]),

$$\mathcal{L}_{\text{REC}} = -\mathbb{E}_{\mathbf{z} \sim q_\phi(\mathbf{z}|\mathbf{x}, \mathbf{y})} [\log p_\theta(\mathbf{y}|\mathbf{x}, \mathbf{z})] , \quad (1)$$

$$\mathcal{L}_{\text{KL}} = D_{\text{KL}}(q_\phi(\mathbf{z}|\mathbf{x}, \mathbf{y}) \| p_\gamma(\mathbf{z}|\mathbf{x})) . \quad (2)$$

The term in Eq. (1) promotes consistency between the decoder output and the observed ground truth, while Eq. (2) brings the posterior and prior distributions together by minimizing their Kullback-Leibler (KL) divergence. In practice, K samples \mathbf{z}_k from q_ϕ are drawn and a deterministic decoder function f_θ maps each $(\mathbf{x}, \mathbf{z}_k)$ pair to an output trajectory

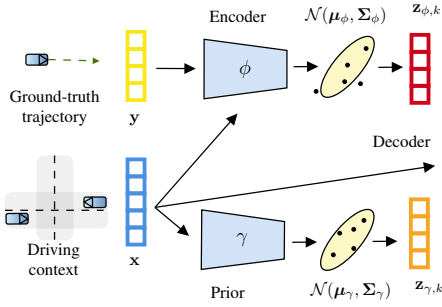


Fig. 2: CVAE: in training, the model captures the joint distribution of the ground-truth trajectory and driving context via the encoder network ϕ , samples randomly, and reconstructs trajectories via the decoder network θ . In inference, the prior network γ replaces ϕ and is sampled instead.

$y_k = f_\theta(\mathbf{x}, \mathbf{z}_k)$. Thus, no parametric form of $\mathcal{P}(y|\mathbf{x})$ is estimated and the output distribution is represented by a set of K samples. In this way, the reconstruction term in Eq. (1) can be approximated by the NLL¹ of reconstructed samples y_k under the ground-truth distribution $\mathcal{N}(y, \sigma \mathbf{I})$, yielding

$$\mathcal{L}_{\text{REC-samples}} = -\frac{1}{K} \sum_k \log \mathcal{N}(y_k; y, \sigma \mathbf{I}). \quad (3)$$

A common approximation when predicting entire trajectories in one shot is to assume independence across time steps [26] or a fixed diagonal covariance matrix $\sigma \mathbf{I}$ [40].

2) *Unscented Transform of the Latent Space*: A key component of the CVAE (and its VAE foundation) is random sampling of the latent space. It is a feature of the reparameterization trick [44], employed in order to sample the latent Gaussian posterior and efficiently compute gradients w.r.t. ϕ in Eq. (1). However, it exhibits high variance in training. Therefore, a deterministic-sampling alternative based on the Unscented Transform (UT) [45] (prominent in filtering and control) has emerged in the Unscented Autoencoder (UAE) [7]. It is motivated by the fact that the decoder is a nonlinear function of the posterior distribution. Thus, a set of representative points in the latent space can be chosen and transformed to approximate the output distribution, which is difficult in practice by transforming a few random samples.

The UT application in the VAE context can be straightforwardly extended to the CVAE. The CUAE model is shown in Fig. 3. The model analytically computes the sigma points of the Gaussian posterior $\mathcal{N}(\boldsymbol{\mu}_\phi, \boldsymbol{\Sigma}_\phi)$, $\boldsymbol{\mu}_\phi \in \mathbb{R}^n$. The $2n+1$ sigmas $\{\chi_i\}_{i=0}^{2n}$ are the mean $\chi_n = \boldsymbol{\mu}_\phi$ and a pair on each axis $\chi_{n \pm j} = \boldsymbol{\mu}_\phi \pm \sqrt{n \boldsymbol{\Sigma}_\phi} |_{j, 1 \leq j \leq n}$, where $|_{j}$ indicates the j -th column. For a commonly used diagonal $\boldsymbol{\Sigma}_\phi$, there is no computational overhead since the Cholesky decomposition $\sqrt{\boldsymbol{\Sigma}_\phi}$ can be directly obtained from predicted log variances.

Since the sigmas fully describe the latent distribution², they usually also describe the output distribution well w.r.t commonly used decoder nonlinearities [46]. Thus, going one step further, we can approximate the expectation in Eq. (1) by the mean of the transformed sigmas. With this, we push the entire output distribution (w.r.t. its mean) toward the ground

¹In image modeling, it is usually the Mean Squared Error (MSE) instead.

²Their first two moments (the mean and covariance) equal the original distribution's first two moments.

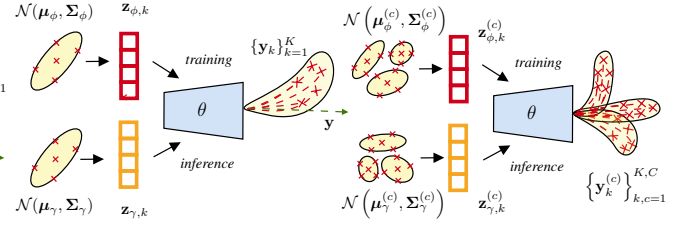


Fig. 3: CUAE: instead of sampling the latent space randomly (in both training and inference), the model analytically computes sigma points of the ϕ and γ distributions and transforms them instead.

Fig. 4: GMM-CUAE: it structures the latent space into a GMM and separately transforms its components (sigma points shown). Compared to Fig. 3, it has the potential to better model multi-modality.

truth instead of the individually transformed samples. Thus,

$$\mathcal{L}_{\text{REC-dist}} = -\log \mathcal{N}\left(\frac{1}{K} \sum_k \mathbf{y}_k; \mathbf{y}, \sigma \mathbf{I}\right), \quad (4)$$

where each \mathbf{y}_k comes from a latent space sigma point. In practice, due to a large dimensionality n , we select $K < 2n+1$ random pairs of sigma points on the same covariance axis [7].

In the context of trajectory prediction, sigma points have the potential to reasonably cover the latent space with few samples, train the entire output distribution accordingly, and prevent spurious and unlikely samples in inference.

B. Latent Space Structure and Inference Strategy

Many use-cases within probabilistic trajectory prediction necessitate a disjoint output with well-separated modes such as turning left or right. Here, CVAEs struggle due to the continuous latent distribution that is decoded as a continuous distribution of trajectories. Therefore, we propose two methods to promote a multi-modal output space. Both use a GMM structure: the first imposes it to the latent space and the second uses a separately-constructed GMM purely for inference.

1) *GMM Latent Space*: The mixture prior model attempts to capture distinct modes of behavior using a GMM for the prior and posterior distributions in the latent space, see Fig. 4. The GMM components can correspond with modes of behavior, while the distribution of each can represent the variation within each mode. For example, one mode may correspond to a right-turn behavior whose speed or path variation is given by the variance. The two GMMs with C components are described by $\sum_c w_\phi^{(c)} \mathcal{N}(\boldsymbol{\mu}_\phi^{(c)}, \boldsymbol{\Sigma}_\phi^{(c)})$ and $\sum_c w_\gamma^{(c)} \mathcal{N}(\boldsymbol{\mu}_\gamma^{(c)}, \boldsymbol{\Sigma}_\gamma^{(c)})$, for fixed C . Sampling is performed independently for each component; we draw K random samples or sigma points from each, totaling $K \cdot C$. Then, we compute the centroid $\mathbf{y}_\mu^{(c)}$ and covariance $\mathbf{y}_\Sigma^{(c)}$ of the decoded trajectories for each mode to obtain an output-space GMM, with the corresponding component weights carried over.

The loss functions in Eq. (1) and Eq. (2) are adapted as follows to be compatible with a GMM representation. As the KL divergence between Gaussian mixtures is not analytically defined, we apply it individually (according to Eq. (2)) between each corresponding posterior and prior component and their discrete mixture distributions

$$\mathcal{L}_{\text{KL-GMM}} = \sum_c \mathcal{L}_{\text{KL}}^{(c)} + D_{\text{KL}}(w_\phi \| w_\gamma). \quad (5)$$

The reconstruction loss minimizes the NLL of the ground-truth trajectory under the predicted future distribution, repre-

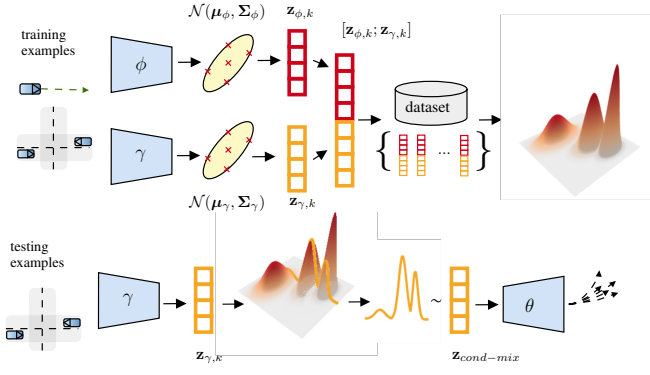


Fig. 5: Illustration of conditional ex-post (CXP) joint mixture construction and conditional sampling. Top: all posterior and prior sigma points in training are concatenated, collected, and used to fit a mixture. Bottom: given a new example’s prior encoding, the mixture is conditioned (intuitively, it is “cut”). The resulting lower-dim. mixture is sampled as input for the decoder.

sented by the output GMM. This way, we train the component whose centroid trajectory is closest to the ground-truth \mathbf{y} (denoted by c^*) and a corresponding one-hot distribution $w_{\mathbf{y}}$ of the closest component,

$$\mathcal{L}_{\text{REC-GMM}} = -\log \mathcal{N}(\mathbf{y}; \mathbf{y}_{\mu}^{(c^*)}, \mathbf{y}_{\Sigma}^{(c^*)}) + D_{\text{KL}}(w_{\phi} \| w_{\mathbf{y}}). \quad (6)$$

Note that this form of the reconstruction loss function is closer to the UT-like computation in Eq. (4) than the vanilla CVAE-like computation in Eq. (3), since the likelihood is computed for the centroid trajectory of the winner latent GMM component rather than in expectation over multiple individual latent samples. The choice between random and unscented sampling determines the method to obtain the output trajectories (that approximate the true distribution), which are averaged to compute the centroid.

2) *Conditional Ex-Post (CXP) Estimation*: In this section, we present an alternative to using the trained latent space for inference, which is universal among VAEs and CVAEs. Termed ex-post (XP) estimation, it involves training a latent space but not using it directly in inference. For the VAE, an empirically-obtained distribution constructed after training is sampled instead of the theoretically-imposed standard normal prior [47]. The advantage is that it addresses the well-known VAE posterior mismatch³ as well as enables deterministic autoencoders (lacking a probabilistic latent space) to generate samples. It can be realized by collecting a dataset of posterior encodings during training $\mathcal{D}_{\text{ex-post}} = \{\mathbf{z}_{\phi}^i\}$ (i for training example) and using an off-the-shelf tool (e.g. [48]) to fit another more expressive distribution. For example, a GMM with C Gaussians, $p(\mathbf{z}_{\phi\text{mix}}) = \sum_c w^{(c)} \mathcal{N}(\mathbf{z}_{\phi\text{mix}}; \boldsymbol{\mu}_{\phi\text{mix}}^{(c)}, \boldsymbol{\Sigma}_{\phi\text{mix}}^{(c)})$, where $\mathbf{z}_{\phi\text{mix}}$ is the GMM random variable, $w^{(c)}$ are the obtained weights, and C is a priori defined. This empirical distribution is then sampled instead.

We extend the original method to the CVAE and CUAE by introducing a conditional ex-post (CXP) estimated density. The vanilla XP sampling is inadequate in the CVAE case since using a mixture built only from the posterior encodings \mathbf{z}_{ϕ} precludes conditioning, e.g. the driving context encoun-

tered in a test set example. Therefore, we incorporate the prior encoding \mathbf{z}_{γ} (obtained through the conditional prior γ , see Fig. 2). First, we collect a set of concatenated posterior-prior pairs $\mathcal{D}_{\text{cond-ex-post}} = \{\mathbf{z}_{\phi}^i; \mathbf{z}_{\gamma}^i\}$ and then fit a GMM $p(\mathbf{z}_{\phi\gamma\text{mix}})$. See Fig. 5 (top) for an illustration. These pairs are a dataset of latent-space relationships between future trajectories and the associated context. Thus, concatenating them and fitting a GMM models the joint distribution between the ground-truth-future-posterior and the context-prior that preceded it. However, sampling given a new context \mathbf{x} requires conditioning the joint mixture on \mathbf{z}_{γ} . In the following, we lay out the necessary steps.

Assume that the mixture of posterior-prior encodings is parameterized by C Gaussians along with their weights $w^{(c)}$

$$p(\mathbf{z}_{\phi\gamma\text{mix}}) = \sum_c w^{(c)} \mathcal{N}(\mathbf{z}_{\phi\gamma\text{mix}}; \boldsymbol{\mu}_{\phi\gamma\text{mix}}^{(c)}, \boldsymbol{\Sigma}_{\phi\gamma\text{mix}}^{(c)}). \quad (7)$$

The random variable realization $\mathbf{z}_{\phi\gamma\text{mix}}$ can be split into $\mathbf{z}_{\phi\gamma\text{mix}} = [\mathbf{z}_1; \mathbf{z}_2]$, $\dim(\mathbf{z}_1) = \dim(\mathbf{z}_{\phi})$ and $\dim(\mathbf{z}_2) = \dim(\mathbf{z}_{\gamma})$. Note that \mathbf{z}_1 and \mathbf{z}_2 “belong” to $p(\mathbf{z}_{\phi\gamma\text{mix}})$ and are not the same as \mathbf{z}_{ϕ} and \mathbf{z}_{γ} . Thus, each component c is factored as

$$\boldsymbol{\mu}_{\phi\gamma\text{mix}}^{(c)} = \begin{bmatrix} \boldsymbol{\mu}_1^{(c)} \\ \boldsymbol{\mu}_2^{(c)} \end{bmatrix}, \quad \boldsymbol{\Sigma}_{\phi\gamma\text{mix}}^{(c)} = \begin{bmatrix} \boldsymbol{\Sigma}_{11}^{(c)} & \boldsymbol{\Sigma}_{12}^{(c)} \\ \boldsymbol{\Sigma}_{21}^{(c)} & \boldsymbol{\Sigma}_{22}^{(c)} \end{bmatrix}. \quad (8)$$

The aim is to compute the conditional mixture distribution $p(\mathbf{z}_1 | \mathbf{z}_2) = \frac{p(\mathbf{z}_1, \mathbf{z}_2)}{p(\mathbf{z}_2)}$. In [49], the conditional distribution of a component in a multivariate Gaussian is given by

$$\mathcal{N}(\mathbf{z}_1 | \mathbf{z}_2; \boldsymbol{\mu}_{\phi\gamma\text{mix}}^{(c)}, \boldsymbol{\Sigma}_{\phi\gamma\text{mix}}^{(c)}) = \mathcal{N}(\mathbf{z}_1; \boldsymbol{\mu}_{1|2}^{(c)}, \boldsymbol{\Sigma}_{1|2}^{(c)}), \quad (9)$$

$$\boldsymbol{\mu}_{1|2}^{(c)} = \boldsymbol{\mu}_1^{(c)} + \boldsymbol{\Sigma}_{12}^{(c)} (\boldsymbol{\Sigma}_{22}^{(c)})^{-1} (\mathbf{z}_2 - \boldsymbol{\mu}_2^{(c)}), \quad (10)$$

$$\boldsymbol{\Sigma}_{1|2}^{(c)} = \boldsymbol{\Sigma}_{11}^{(c)} - \boldsymbol{\Sigma}_{12}^{(c)} (\boldsymbol{\Sigma}_{22}^{(c)})^{-1} \boldsymbol{\Sigma}_{21}^{(c)}. \quad (11)$$

The marginal distribution $p(\mathbf{z}_2)$ is given simply by $\sum_c w^{(c)} \mathcal{N}(\mathbf{z}_2; \boldsymbol{\mu}_{22}^{(c)}, \boldsymbol{\Sigma}_{22}^{(c)})$. Thus, $p(\mathbf{z}_1 | \mathbf{z}_2)$ is computed by

$$p(\mathbf{z}_1 | \mathbf{z}_2) = \sum_c \frac{w^{(c)} \mathcal{N}(\mathbf{z}_2; \boldsymbol{\mu}_{22}^{(c)}, \boldsymbol{\Sigma}_{22}^{(c)})}{p(\mathbf{z}_2)} \mathcal{N}(\mathbf{z}_1; \boldsymbol{\mu}_{1|2}^{(c)}, \boldsymbol{\Sigma}_{1|2}^{(c)}), \quad (12)$$

where the fraction provides the new mixture weights that are normalized by the density of the marginal $p(\mathbf{z}_2)$. In this manner, we can sample $\mathbf{z}_{\text{cond-mix}} \sim p(\mathbf{z}_1 | \mathbf{z}_2 = \mathbf{z}_{\gamma})$ and feed the decoder with $\mathbf{z}_{\text{cond-mix}}$ instead of \mathbf{z}_{γ} , $p_{\theta}(\mathbf{y} | \mathbf{x}, \mathbf{z}_{\text{cond-mix}})$. Thus, $p(\mathbf{z}_1 | \mathbf{z}_2)$ serves as a link to obtain a latent vector close to what would be a posterior encoding (through their joint mixture relationship), considering that the posterior is not available in inference. See Fig. 5 (bottom) for an illustration.

The conditional mixture in Eq. (12) provides a more expressive sampling distribution than the simplistic Gaussian prior. The conditioning by the prior sample results in a distribution that contains similar ground-truth training posteriors. Further, the weights of the conditional mixture (the fraction in Eq. (12)), different to $w^{(c)}$ in Eq. (7), can effectively prune irrelevant components by assigning low values, potentially providing $\ll C$ components with non-negligible weights. In this way, a variable number of components in the latent space can be modeled based on the encountered context.

In the context of the CXP-CUAE model, an open question is choosing the specific \mathbf{z}_{γ} vector to condition the joint

³In practice, the average posterior over the entire training set does not fully match the assumed $\mathcal{N}(\mathbf{0}, \mathbf{I})$ prior, leading to lower sample quality.

mixture. Considering that the prior γ can provide sigma points, each of the $2n+1$ distinct points would result in a different conditional mixture. We choose the sigma point that incurs the largest density in the marginal distribution $p(\mathbf{z}_2)$ (the denominator term in Eq. (12)). Intuitively, such a sigma point would cut the joint mixture where it is most data-rich.

C. Output Trajectory Generation

Commonly used metrics such as Minimum Average Displacement Error (minADE) and Minimum Final Displacement Error (minFDE) (see [26] for definitions) necessitate a fixed number of M candidate trajectories, e.g. $M=6$. CVAEs inherently exhibit large variance on such metrics due to the random sampling. Even the deterministic sampling of the CUAE poses the question of which M sigmas to provide among $2n+1$ choices, $M \ll 2n+1$. Therefore, we investigate a simple way to provide a more consistent output. We first draw a large number of K random samples (CVAE) or take all $K=2n+1$ latent sigmas (CUAE). Then, we cluster them into M clusters with a k-means procedure and provide only the centroids. A similar approach is explored in [20]. Thus, we also evaluate the clustering-enhanced CVAE, CUAE, and the CXP-CUAE, detailed in Sec. III-A.1, III-A.2, and III-B.2, respectively. We do not apply it to the latent space GMM from Sec III-B.1 since it already has a mechanism to provide fixed M trajectories through the $C=M$ components. We expect that this approach especially boosts the performance of the CUAE in training, since it translates its structured latent space coverage into the output space. Overall, as we offer multiple models touching different facets of the CVAE, we summarize our proposed approaches in Tab. I (left).

IV. RESULTS

Here, we describe the experimental setup and present the results of our proposed CVAE trajectory prediction models. As CVAEs are used beyond this task, our architectural improvements are not limited to prediction, which is the primary evaluation setting. Thus, to better understand our models, we extend the evaluation with the secondary setting of classical image modeling on the rich CelebA [50] dataset.

A. Implementation

The network architectures of our CVAE approaches explicitly follow the StarNet model [16]. It is a deterministic, single-agent⁴ predictor that uses a graph-based map and trajectory history context. We use a shared StarNet encoder, comprising a 1D-CNN trajectory history network, GNN map network and an attention-based [51] agent interaction network as a basis for the posterior ϕ and prior γ distributions. Since the posterior ϕ additionally receives the ground-truth future trajectory, we reuse the 1D-CNN. Thus, in both ϕ and γ the StarNet encoder produces a single feature vector passed onto a two-layer [128, 128] MLP with batch normalization and ReLU activation. The output of this MLP is passed onto two separate 32-dim. layers producing $\boldsymbol{\mu}_\phi$ or $\boldsymbol{\mu}_\gamma$ and $\log \sigma_\phi^2$

⁴Our CVAE-level improvements have no inherent restrictions toward a joint prediction extension, which is a more sound approach to the problem.

or $\log \sigma_\gamma^2$ (used to construct diagonal covariance matrices). In the GMM-CVAE⁵ in Sec. III-B.1, an additional 64-dim. layer produces weights w_ϕ or w_γ from concatenated means and variances as input. The StarNet decoder θ predicts future trajectories in an action-based manner⁶ [53]. We emphasize that other more sophisticated models can be used within the encoder/decoder, which is orthogonal to our top-level CVAE.

In image modeling experiments, we use the identical setup from [7] and extend it with a prior γ network. It encodes the conditioning \mathbf{x} in the CelebA dataset consisting of a 40-dim. binary vector of face attributes (whereas the ground-truth \mathbf{y} acc. to Fig. 2 is an image). The prior γ is realized as a [64, 64] MLP for both $\boldsymbol{\mu}_\gamma$ and $\log \sigma_\gamma^2$ with a shared first layer.

B. Datasets and Training Setup

We trained and evaluated our trajectory prediction models on the INTERACTION [54] dataset of highly interactive driving containing merges, roundabouts, and intersections. We used the official training and validation splits, predicting 3s trajectories ($T=30$ at 10Hz) given a 1s history. In image modeling, we used the rich CelebA dataset [50] of human faces, containing $64 \times 64 \times 3$ images pre-processed the same way as in [7] and 40-dim. binary attribute annotations⁷.

The prediction models are trained for 30 epochs with Adam [55], starting from a $1e^{-4}$ learning rate and halving it for epochs 10, 15, 20, and 25. CelebA experiments use the same setup as in [7]: 100 epochs and a learning rate halving on loss plateau. All models are implemented in PyTorch [56]. In CXP estimation, we used [57] (compatible with [48]) for fast GPU-based GMM fitting after training, taking around 30 min. over the entire training set. In both use-cases, the models took around 1.5 days to train on a single Nvidia 3090 GPU.

C. Image Modeling Performance

In this secondary evaluation setting, our aim is to assess the proposed models' ability to generate realistic images. One goal is reconstructing existing images by compressing and decompressing them from the latent space (a task trajectory prediction models are not evaluated on). More specifically, a trained CVAE encodes a ground-truth image \mathbf{y} and its attributes as context \mathbf{x} into the posterior distribution $\mathcal{N}(\mathbf{z}_\phi | \mathbf{x}, \mathbf{y}; \boldsymbol{\mu}_\phi, \boldsymbol{\Sigma}_\phi)$. Then, it feeds a random sample (or sigma) $\mathbf{z}_{\phi,k}$ to the decoder, which reconstructs the output image $\mathbf{y}_k = f_\theta(\mathbf{x}, \mathbf{z}_{\phi,k})$. This process is conceptually the same as the CVAE in Fig. 2. Furthermore, we evaluate the ability to generate realistic new image samples. In this manner, the model only receives the context \mathbf{x} encoded into the prior $\mathcal{N}(\mathbf{z}_\gamma | \mathbf{x}; \boldsymbol{\mu}_\gamma, \boldsymbol{\Sigma}_\gamma)$. Then, the decoder produces an image

⁵The term GMM-CVAE was previously used in [42] in a prediction context and in [52] in image modeling. The former uses a categorical latent space and regresses an output-level GMM. The latter uses pre-defined clusters as modes of the GMM, where cluster labels are already available instead of being learned in the training process. Since both approaches significantly differ from ours, we reuse the term for our latent-space GMM.

⁶The model first predicts future actions (acceleration and steering angle) and then unrolls them into future positions (starting from the current position) using a kinematic bicycle model.

⁷Examples include: *Smiling, Eyeglasses, Young, Blond_Hair*.

Model	sampling	latent space	inference via	K	M	minADE	minFDE	mixture-NLL			winner-NLL		
								1s	2s	3s	1s	2s	3s
CVAE	random	Gaussian	latent space	6	6	0.149	0.478	-	-	-	1.846	1.877	2.167
CVAE	random	Gaussian	latent space	65	65	0.078	0.209	-	-	-	1.845	1.854	1.955
CUAE	unscented	Gaussian	latent space	6	6	0.145	0.452	-	-	-	1.846	1.872	2.131
CUAE	unscented	Gaussian	latent space	65 (all)	65	0.087	0.170	-	-	-	1.845	1.846	1.899
CVAE+clusters	random	Gaussian	latent space	65	6	0.134	0.454	1.842	1.928	2.607	-2.685	-0.382	1.980
CUAE+clusters	unscented	Gaussian	latent space	65 (all)	6	0.130	0.400	1.850	2.010	2.780	-2.701	-1.358	1.011
CXP-CVAE+clusters	random	Gaussian	cond. ex-post	65	6	0.128	0.427	-2.556	3.400	6.608	-	-	-
CXP-CUAE+clusters	unscented	Gaussian	cond. ex-post	65 (all)	6	0.122	0.379	-2.431	0.336	2.792	-	-	-
GMM-CVAE	random	GMM	latent space	65	6	0.101	0.301	-0.437	-0.016	1.152	-	-	-
GMM-CUAE	unscented	GMM	latent space	65 (all)	6	0.097	0.283	-0.430	0.053	1.150	-	-	-

TABLE I: Left half: Breakdown of the approaches described in Sec. III. Note that all of the approaches in the gray-colored rows below the CVAE rows are proposed in this work. Right half: Corresponding INTERACTION experiment results. Legend: K – number of samples/sigmas from the latent space (6 or 65 due to a 32-dim. latent space), M – number of final provided trajectories, +clusters – K decoded samples/sigmas in the output are clustered into M trajectories, GMM latent space – M trajectories are given by the centroids of K decoded samples/sigmas per each GMM component.

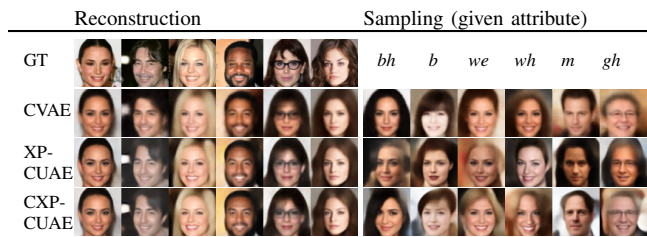


Fig. 6: Example reconstructed and sampled images (best viewed in color and zoomed in). The XP-CUAE and CXP-CUAE inference models generate sharper images than vanilla CVAE, as also evidenced by the quantitative results of corresponding rows in Tab. II. Furthermore, the proposed CXP inference succeeds at incorporating the attributes into samples, while the baseline XP inference struggles with it. Attributes: *Black_Hair* (*bh*), *Bangs* (*b*), *Wearing_Earrings* (*we*), *Wavy_Hair* (*wh*), *Male* (*m*), *Gray_Hair* (*gh*).

$\mathbf{y}_k = f_\theta(\mathbf{x}, \mathbf{z}_{\gamma,k})$ using a sample $\mathbf{z}_{\gamma,k}$. In contrast, the CXP-CVAE produces an image in inference using a sample from the conditional mixture, $\mathbf{y}_k = f_\theta(\mathbf{x}, \mathbf{z}_{\text{cond-mix}})$. For all models, we use four samples (or random sigmas) in training. In both reconstruction and sampling, we evaluate image realism with the established Fréchet Inception Distance (FID) [58], which computes the Wasserstein metric between sets of real and sampled images.

Tab. II shows quantitative results comparing the vanilla CVAE, CUAE, and both with CXP estimation ($C=10$, see Eq. (7)). We do not include GMM-CVAE since generating multiple image outputs is usually not relevant to the problem (which is stationary). We additionally ablate the baseline XP estimation from [7], [47], which does not condition on attributes \mathbf{x} ; it fits the mixture only on $\mathbf{z}_{\phi,k}$ and directly samples $\mathbf{z}_{\phi,\text{mix}}$ to feed the decoder $\mathbf{y}_k = f_\theta(\mathbf{x}, \mathbf{z}_{\phi,\text{mix}})$. We observe that the best scores are achieved by CUAE models with (C)XP estimation. Fig. 6 qualitatively corroborates the results from Tab. II; it is evident that such models generate sharper and more realistic images than prior inference models. As expected though, the XP-CVAE struggles to include the queried attribute into the image (since the sample $\mathbf{z}_{\phi,\text{mix}}$ does not contain it), something vanilla CVAE and our CXP-CVAE are well capable of.

D. Trajectory Prediction Performance

In this section, we pit our proposed CVAE improvements against each other: CUAE (Sec. III-A.2), GMM latent space (Sec. III-B.1), CXP (Sec. III-B.2), as well as output-level

Model	sampling	inference via	image modeling	
			reconstr.	sampling
CVAE	random	latent space	59.74	62.61
CUAE	unscented	latent space	47.92	98.50
XP-CVAE	random	ex-post	59.29	63.70
XP-CUAE	unscented	ex-post	40.67	48.83
CXP-CVAE	random	cond. ex-post	59.32	63.53
CXP-CUAE	unscented	cond. ex-post	40.44	48.52

TABLE II: Quantitative image modeling results on FID (lower is better). We ablate the proposed unscented sampling, ex-post estimation (XP) [47], [7], and the proposed conditional ex-post estimation (CXP).

Model	minADE ₆	minFDE ₆
ITRA [59]	0.17	0.49
GOHOME [12]	-	0.45
joint-StarNet [16]	0.13	0.38
DiPA [26]	0.11	0.34
MB-SS-ASP [60]	0.10	0.30
SAN [61]	0.10	0.29
GMM-CUAE	0.097	0.283

TABLE III: Comparison of the best model in Tab. I with models from the literature on the INTERACTION validation dataset.

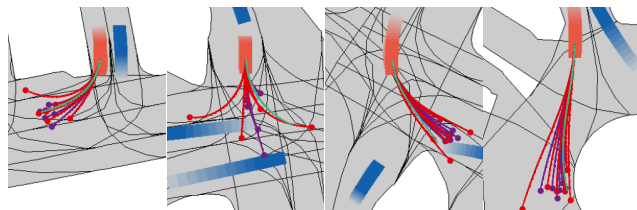


Fig. 7: Qualitative comparison of sampling choices (best viewed in color): trajectories reconstructed from sigma points (red) are significantly more diverse than random samples (purple). Traffic participants are depicted in blue and the predicted vehicle in red, with fading for history.

clustering (Sec. III-C) on the primary, trajectory prediction evaluation setting. We aim to evaluate the quality of multi-modal predictions on a trajectory and distribution level using the minADE and minFDE metrics as well as the distributional NLL. Comprehensive results are shown in Tab. I (right). Since our approaches relate to core CVAE aspects, our main baseline is a vanilla CVAE, however, Tab. III shows a comparison of our highest-performing model with non-CVAE approaches in literature.

The first four rows of Tab. I show the results of CVAE and CUAE models from Sec. III-A. We trained with $\sigma=1.0$ in Eq. (3) and Eq. (4) (it has been shown to work well for sample-based predictors [40]). Since it is nontrivial to compute the full NLL, we compute it only for the closest

mode to the ground truth ($\sigma=1.0$). We see that the CUAE provides a 5% boost over CVAE in trajectory metrics, however, qualitative results in Fig. 7 show the potential of sigma points to provide good coverage, as illustrated in Fig. 1. Further, both CVAE and CUAE benefit from increasing the number of samples or using all sigma points (32-dim. latent space yields $K=65$), though these models are not comparable with the rest. The output clustering from Sec. III-C provides $M=6$ trajectories based on the K samples/sigmas. It especially benefits the CUAE; its thorough output-space coverage is encapsulated into few higher quality candidates than the CVAE's clustered outputs. The $>50\%$ lower winner-NLL (only the cluster centroid closest to the ground truth is evaluated) shows that clusters on sigma trajectories are more meaningful. However the mixture-NLL, computed using ratios of members in each cluster as weights, is high. It shows that such weights are not a good proxy for the actual mixture distribution.

CXP provides an alternative to the latent prior in inference. We apply it to the clustering models in which we fit a $C=50$ -component GMM from the training set posterior and prior encodings after training. Then, we condition it as described in Sec. III-B.2 and draw $K=65$ samples from the conditional mixture, clustered into $M=6$ trajectories. CXP brings additional gains in trajectory metrics, showing that a more expressive inference distribution is beneficial. However, it does not provide an easy way to compute the mixture NLL. We approximate it via the conditional mixture weights and component mean sigma trajectories. Finally, the GMM latent model (with $C=M=6$) provides the best scores, significantly outperforming the previous models in trajectory- and distribution-level metrics. It shows that inducing a more expressive latent space in a CVAE context (while accordingly approximating the ELBO) brings significant performance improvements. Here, random and unscented sampling perform similarly well. However, it is important to note that the GMM reconstruction loss function in Eq. (6) already incorporates a crucial aspect of the UT, as described in Sec. III-A.2. The reconstruction error is computed in a CUAE-like manner (see Eq. (4)), using the likelihood of the centroid trajectory of the winner GMM component (where the centroid is computed either by transforming random samples or sigmas), rather than in a CVAE-like manner (see Eq. (3)), using the expectation of individually reconstructed trajectories.

Overall, the obtained results comprehensively demonstrate the efficacy of our proposed alternatives to key components of the trajectory prediction CVAE, answering the research questions (i) and (ii) posed in Sec. I. First, the unscented sampling and latent space transformation can bring greater diversity in output trajectories while outperforming the ubiquitous random sampling. Second, alternative inference procedures, validated in non-prediction contexts as well, can utilize substantially more expressive distributions to draw higher-quality samples, while requiring no training overhead. Finally, greatest advantages can be found in directly training a more expressive Gaussian mixture latent space whose components map to a structured multi-modal output distribution.

V. CONCLUSION

In this paper, we investigated important shortcomings of the CVAE in trajectory prediction. We answered questions surrounding latent space assumptions by showing that unscented sampling and mixture models in training and inference provide high performance alternatives to existing structures. We anticipate that our findings will lead to a more effective usage of CVAE models in prediction and beyond.

REFERENCES

- [1] B. Ivanovic, K. Leung, E. Schmerling, and M. Pavone, "Multimodal Deep Generative Models for Trajectory Prediction: A Conditional Variational Autoencoder Approach," *IEEE Robotics and Automation Letters*, 2020.
- [2] T. Salzmann, B. Ivanovic, P. Chakravarty, and M. Pavone, "Trajectron++: Dynamically-feasible Trajectory Forecasting with Heterogeneous Data," in *Computer Vision—ECCV 2020: 16th European Conference, Glasgow, UK, August 23–28, 2020, Proceedings, Part XVIII 16*. Springer, 2020.
- [3] S. Casas, C. Gulino, S. Suo, K. Luo, R. Liao, and R. Urtasun, "Implicit Latent Variable Model for Scene-consistent Motion Forecasting," in *Computer Vision—ECCV 2020: 16th European Conference, Glasgow, UK, August 23–28, 2020, Proceedings, Part XXIII 16*. Springer, 2020.
- [4] A. Cui, S. Casas, A. Sadat, R. Liao, and R. Urtasun, "LookOut: Diverse Multi-future Prediction and Planning for Self-driving," in *Proceedings of the IEEE/CVF International Conference on Computer Vision*, 2021.
- [5] Y. Yuan, X. Weng, Y. Ou, and K. M. Kitani, "Agentformer: Agent-aware Transformers for Socio-temporal Multi-agent Forecasting," in *Proceedings of the IEEE/CVF International Conference on Computer Vision*, 2021.
- [6] M. Lee, S. S. Sohn, S. Moon, S. Yoon, M. Kapadia, and V. Pavlovic, "Muse-VAE: Multi-scale VAE for Environment-aware Long Term Trajectory Prediction," in *Proceedings of the IEEE/CVF Conference on Computer Vision and Pattern Recognition*, 2022.
- [7] F. Janjoš, L. Rosenbaum, M. Dolgov, and J. M. Zöllner, "Unscented Autoencoder," in *40th International Conference on Machine Learning (ICML)*, 2023.
- [8] J. Gao, C. Sun, H. Zhao, Y. Shen, D. Anguelov, C. Li, and C. Schmid, "VectorNet: Encoding Hd Maps and Agent Dynamics From Vectorized Representation," in *Proceedings of the IEEE/CVF Conference on Computer Vision and Pattern Recognition*, 2020.
- [9] H. Cui, T. Nguyen, F.-C. Chou, T.-H. Lin, J. Schneider, D. Bradley, and N. Djuric, "Deep Kinematic Models for Kinematically Feasible Vehicle Trajectory Predictions," in *2020 IEEE International Conference on Robotics and Automation (ICRA)*. IEEE, 2020.
- [10] T. Gilles, S. Sabatini, D. Tsishkou, B. Stanciulescu, and F. Moutarde, "HOME: Heatmap Output for Future Motion Estimation," in *2021 IEEE International Intelligent Transportation Systems Conference (ITSC)*. IEEE, 2021.
- [11] H. Zhao, J. Gao, T. Lan, C. Sun, B. Sapp, B. Varadarajan, Y. Shen, Y. Shen, Y. Chai, C. Schmid, *et al.*, "TNT: Target-driven Trajectory Prediction," in *Conference on Robot Learning*. PMLR, 2021.
- [12] T. Gilles, S. Sabatini, D. Tsishkou, B. Stanciulescu, and F. Moutarde, "GOHOME: Graph-oriented Heatmap Output for Future Motion Estimation," in *2022 international conference on robotics and automation (ICRA)*. IEEE, 2022.
- [13] M. Liang, B. Yang, R. Hu, Y. Chen, R. Liao, S. Feng, and R. Urtasun, "Learning Lane Graph Representations for Motion Forecasting," in *Computer Vision—ECCV 2020: 16th European Conference, Glasgow, UK, August 23–28, 2020, Proceedings, Part II 16*. Springer, 2020.
- [14] T. Gilles, S. Sabatini, D. Tsishkou, B. Stanciulescu, and F. Moutarde, "THOMAS: Trajectory Heatmap Output with Learned Multi-agent Sampling," *arXiv preprint arXiv:2110.06607*, 2021.
- [15] J. Ngiam, V. Vasudevan, B. Caine, Z. Zhang, H.-T. L. Chiang, J. Ling, R. Roelofs, A. Bewley, C. Liu, A. Venugopal, *et al.*, "Scene Transformer: A Unified Architecture for Predicting Future Trajectories of Multiple Agents," in *International Conference on Learning Representations*, 2021.
- [16] F. Janjoš, M. Dolgov, and J. M. Zöllner, "StarNet: Joint Action-space Prediction with Star Graphs and Implicit Global-frame Self-attention," in *2022 IEEE Intelligent Vehicles Symposium (IV)*. IEEE, 2022.

- [17] A. Cui, S. Casas, K. Wong, S. Suo, and R. Urtasun, "GoReLa: Go Relative for Viewpoint-invariant Motion Forecasting," in *2023 IEEE International Conference on Robotics and Automation (ICRA)*. IEEE, 2023.
- [18] S. Narayanan, R. Moslemi, F. Pittaluga, B. Liu, and M. Chandraker, "Divide-and-conquer for Lane-aware Diverse Trajectory Prediction," in *Proceedings of the IEEE/CVF Conference on Computer Vision and Pattern Recognition*, 2021.
- [19] J. Gu, C. Sun, and H. Zhao, "DenseTNT: End-to-end Trajectory Prediction From Dense Goal Sets," in *Proceedings of the IEEE/CVF International Conference on Computer Vision*, 2021.
- [20] N. Deo, E. Wolff, and O. Beijbom, "Multimodal Trajectory Prediction Conditioned On Lane-graph Traversals," in *Conference on Robot Learning*. PMLR, 2022.
- [21] M. Hallgarten, I. Kisa, M. Stoll, and A. Zell, "Stay On Track: A Frenet Wrapper to Overcome Off-road Trajectories In Vehicle Motion Prediction," *arXiv preprint arXiv:2306.00605*, 2023.
- [22] Y. Chai, B. Sapp, M. Bansal, and D. Anguelov, "MultiPath: Multiple Probabilistic Anchor Trajectory Hypotheses for Behavior Prediction," *arXiv preprint arXiv:1910.05449*, 2019.
- [23] S. Khandelwal, W. Qi, J. Singh, A. Hartnett, and D. Ramanan, "What-if Motion Prediction for Autonomous Driving," *arXiv preprint arXiv:2008.10587*, 2020.
- [24] T. Phan-Minh, E. C. Grigore, F. A. Boulton, O. Beijbom, and E. M. Wolff, "CoverNet: Multimodal Behavior Prediction Using Trajectory Sets," in *Proceedings of the IEEE/CVF conference on computer vision and pattern recognition*, 2020.
- [25] B. Varadarajan, A. Hefny, A. Srivastava, K. S. Refaat, N. Nayakanti, A. Cornman, K. Chen, B. Douillard, C. P. Lam, D. Anguelov, *et al.*, "MultiPath++: Efficient Information Fusion and Trajectory Aggregation for Behavior Prediction," in *2022 International Conference on Robotics and Automation (ICRA)*. IEEE, 2022.
- [26] A. Knittel, M. Hawasly, S. V. Albrecht, J. Redford, and S. Ramamoorthy, "DiPA: Probabilistic Multi-Modal Interactive Prediction for Autonomous Driving," *IEEE Robotics and Aut. Letters*, 2023.
- [27] N. Rhinehart, R. McAllister, K. Kitani, and S. Levine, "PRECOG: PREdiction Conditioned On Goals In Visual Multi-agent Settings," in *Proceedings of the IEEE/CVF International Conference on Computer Vision*, 2019.
- [28] C. Schöller and A. Knoll, "Flomo: Tractable Motion Prediction with Normalizing Flows," in *2021 IEEE/RSJ International Conference on Intelligent Robots and Systems (IROS)*. IEEE, 2021.
- [29] A. Mészáros, J. Alonso-Mora, and J. Kober, "Trajflow: Learning the Distribution Over Trajectories," *arXiv preprint arXiv:2304.05166*, 2023.
- [30] A. Gupta, J. Johnson, L. Fei-Fei, S. Savarese, and A. Alahi, "Social GAN: Socially Acceptable Trajectories with Generative Adversarial Networks," in *Proceedings of the IEEE conference on computer vision and pattern recognition*, 2018.
- [31] A. Sadeghian, V. Kosaraju, A. Sadeghian, N. Hirose, H. Rezatofighi, and S. Savarese, "Sophie: An Attentive Gan for Predicting Paths Compliant to Social and Physical Constraints," in *Proc. of the IEEE/CVF Conference on Computer Vision and Pattern Recognition*, 2019.
- [32] V. Kosaraju, A. Sadeghian, R. Martín-Martín, I. Reid, H. Rezatofighi, and S. Savarese, "Social-BiGAT: Multimodal Trajectory Forecasting Using Bicycle-GAN and Graph Attention Networks," *Advances in Neural Information Processing Systems*, 2019.
- [33] I. Goodfellow, J. Pouget-Abadie, M. Mirza, B. Xu, D. Warde-Farley, S. Ozair, A. Courville, and Y. Bengio, "Generative Adversarial Networks," *Communications of the ACM*, 2020.
- [34] P. Dendorfer, A. Osep, and L. Leal-Taixé, "Goal-GAN: Multimodal Trajectory Prediction Based On Goal Position Estimation," in *Proceedings of the Asian Conference on Computer Vision*, 2020.
- [35] T. Salimans, I. Goodfellow, W. Zaremba, V. Cheung, A. Radford, and X. Chen, "Improved Techniques for Training GANs," *Advances in neural information processing systems*, 2016.
- [36] U. Tanielián, T. Issenhuth, E. Dohmatob, and J. Mary, "Learning Disconnected Manifolds: a No Gan's Land," in *International Conference on Machine Learning*. PMLR, 2020.
- [37] M. Khayatkhoei, M. K. Singh, and A. Elgammal, "Disconnected Manifold Learning for Generative Adversarial Networks," *Advances in Neural Information Processing Systems*, 2018.
- [38] M. Arjovsky and L. Bottou, "Towards Principled Methods for Training Generative Adversarial Networks," *arXiv preprint arXiv:1701.04862*, 2017.
- [39] M. Arjovsky, S. Chintala, and L. Bottou, "Wasserstein Generative Adversarial Networks," in *International conference on machine learning*. PMLR, 2017.
- [40] P. Dendorfer, S. Elflein, and L. Leal-Taixé, "MG-GAN: A Multi-generator Model Preventing Out-of-distribution Samples In Pedestrian Trajectory Prediction," in *Proceedings of the IEEE/CVF International Conference on Computer Vision*, 2021.
- [41] J. T. Rolfe, "Discrete Variational Autoencoders," *arXiv preprint arXiv:1609.02200*, 2016.
- [42] J. Hong, B. Sapp, and J. Philbin, "Rules of the Road: Predicting Driving Behavior with a Convolutional Model of Semantic Interactions," in *Proceedings of the IEEE/CVF Conference on Computer Vision and Pattern Recognition*, 2019.
- [43] K. Sohn, H. Lee, and X. Yan, "Learning Structured Output Representation Using Deep Conditional Generative Models," *Advances in neural information processing systems*, 2015.
- [44] D. P. Kingma and M. Welling, "Auto-encoding Variational Bayes," *arXiv preprint arXiv:1312.6114*, 2013.
- [45] S. J. Julier and J. K. Uhlmann, "Unscented Filtering and Nonlinear Estimation," *Proceedings of the IEEE*, 2004.
- [46] S. Julier, J. Uhlmann, and H. F. Durrant-Whyte, "A New Method for the Nonlinear Transformation of Means and Covariances In Filters and Estimators," *IEEE Transactions on automatic control*, 2000.
- [47] P. Ghosh, M. S. Sajjadi, A. Vergari, and M. Black, "From Variational to Deterministic Autoencoders," in *8th International Conference on Learning Representations (ICLR)*, 2020.
- [48] F. Pedregosa, G. Varoquaux, A. Gramfort, V. Michel, B. Thirion, O. Grisel, M. Blondel, P. Prettenhofer, R. Weiss, V. Dubourg, J. Vanderplas, A. Passos, D. Cournapeau, M. Brucher, M. Perrot, and E. Duchesnay, "Scikit-learn: Machine Learning In Python," *Journal of Machine Learning Research*, 2011.
- [49] C. M. Bishop and N. M. Nasrabadi, *Pattern Recognition and Machine Learning*. Springer, 2006.
- [50] Z. Liu, P. Luo, X. Wang, and X. Tang, "Deep Learning Face Attributes In the Wild," in *Proceedings of International Conference on Computer Vision (ICCV)*, December 2015.
- [51] A. Vaswani, N. Shazeer, N. Parmar, J. Uszkoreit, L. Jones, A. N. Gomez, Ł. Kaiser, and I. Polosukhin, "Attention Is All You Need," *Advances in neural information processing systems*, 2017.
- [52] L. Wang, A. Schwing, and S. Lazebnik, "Diverse and accurate image description using a variational auto-encoder with an additive gaussian encoding space," *Advances in Neural Information Processing Systems*, vol. 30, 2017.
- [53] F. Janjoš, M. Dolgov, and J. M. Zöllner, "Self-supervised Action-space Prediction for Automated Driving," in *2021 IEEE Intelligent Vehicles Symposium (IV)*. IEEE, 2021.
- [54] W. Zhan, L. Sun, D. Wang, H. Shi, A. Clausse, M. Naumann, J. Kummerle, H. Königshof, C. Stiller, A. de La Fortelle, *et al.*, "Interaction Dataset: An International, Adversarial and Cooperative Motion Dataset In Interactive Driving Scenarios with Semantic Maps," *arXiv preprint arXiv:1910.03088*, 2019.
- [55] D. P. Kingma and J. Ba, "Adam: A Method for Stochastic Optimization," *arXiv preprint arXiv:1412.6980*, 2014.
- [56] A. Paszke, S. Gross, F. Massa, A. Lerer, J. Bradbury, G. Chanan, T. Killeen, Z. Lin, N. Gimelshein, L. Antiga, *et al.*, "PyTorch: An Imperative Style, High-performance Deep Learning Library," *Advances in neural information processing systems*, 2019.
- [57] O. Borchert, "PyCave: Traditional Machine Learning Models for Large-Scale Datasets In PyTorch," <https://github.com/borchero/pycave>, 2022, release used: v3.2.1.
- [58] M. Heusel, H. Ramsauer, T. Unterthiner, B. Nessler, and S. Hochreiter, "GANs Trained by a Two Time-scale Update Rule Converge to a Local Nash Equilibrium," *Advances in neural information processing systems*, 2017.
- [59] A. Scibior, V. Lioutas, D. Reda, P. Bateni, and F. Wood, "Imagining the Road Ahead: Multi-agent Trajectory Prediction Via Differentiable Simulation," in *2021 IEEE International Intelligent Transportation Systems Conference (ITSC)*. IEEE, 2021.
- [60] F. Janjoš, M. Keller, M. Dolgov, and J. M. Zöllner, "Bridging the Gap Between Multi-Step and One-Shot Trajectory Prediction Via Self-Supervision," in *2023 IEEE Intelligent Vehicles Symposium (IV)*. IEEE, 2023.
- [61] F. Janjoš, M. Dolgov, M. Kurić, Y. Shen, and J. M. Zöllner, "SAN: Scene Anchor Networks for Joint Action-Space Prediction," in *2022 IEEE Intelligent Vehicles Symposium (IV)*. IEEE, 2022.